Orthogonal spin arrangement as possible ground state of three-dimensional Shastry-Sutherland network in $Ba_3Cu_3In_4O_{12}$

O. S. Volkova,[1] I. S. Maslova,[1] R. Klingeler,[2] M. Abdel-Hafiez,[3] Y. C. Arango,[3] A. U. B. Wolter,[3] V. Kataev,[3] B. Büchner,[3] and A. N. Vasiliev[1]

[1]*Low Temperature Physics and Superconductivity Department, M.V. Lomonosov Moscow State University, Moscow 119991, Russia*

[2]*Kirchhoff Institute for Physics, University of Heidelberg, D-69120 Heidelberg, Germany*

[3]*Leibniz Institute for Solid State and Materials Research, IFW Dresden, D-01069 Dresden, Germany*

(Received 1 October 2011; revised manuscript received 1 February 2012; published 30 March 2012)

The $Ba_3Cu_3In_4O_{12}$ stands for unique topology of the magnetic subsystem. It consists of rotated by 90° relative to each other "paper-chain" columns made of vertex-sharing Cu^IO_4 and $Cu^{II}O_4$ planar units. The overall pattern of the copper ions is that of a three-dimensional Shastry-Sutherland network. At high temperatures, the magnetic susceptibility follows the Curie-Weiss law with positive Weiss temperature indicating strong predominance of ferromagnetic coupling. At low temperatures, however, this compound exhibits a long-range antiferromagnetically ordered state that reaches saturation magnetization by a nontrivial succession of two spin-flop and two spin-flip transitions already in modest magnetic fields. We show that the ground state in $Ba_3Cu_3In_4O_{12}$ may be a three-dimensional orthogonal arrangement of the Cu^{2+} ($S = 1/2$) magnetic moments forming three virtually independent antiferromagnetic subsystems. In this arrangement, favored by anisotropic exchange interactions, the quantum fluctuations provide the coupling between three mutually orthogonal magnetic subsystems resulting in an impressive "order by disorder" effect.

DOI: 10.1103/PhysRevB.85.104420 PACS number(s): 75.10.−b, 75.30.Et, 75.40.Cx, 75.47.Lx

I. INTRODUCTION

Low-dimensional and frustrated magnetic systems have shown to attract attention by their rich variety of quantum ground states realized at low temperatures. Fascinating examples for exotic states are spin liquids and various types of long-range collinear and noncollinear magnetic structures. Famous spin liquids are the ancient Han-Purple pigment $BaCuSi_2O_6$,[1] the spin-Peierls compound $CuGeO_3$,[2] the Haldane chain Y_2BaNiO_5,[3] and the Shastry-Sutherland network $SrCu_2(BO_3)_2$.[4] Representatives of noncollinear magnetic structures are helixes in quasi-one-dimensional quantum spin systems $LiCu_2O_2$,[5] $LiCuVO_4$,[6] and Li_2ZrCuO_4[7] where the arrangement of adjacent magnetic moments is a compromise between several isotropic superexchange interactions.[8] The pitch angle in these helixes depends on the ratio between magnetic nearest-neighbor and next-nearest-neighbor exchange interactions being close to 90° in a wide range of parameters.[9] There exists, however, another class of low-dimensional antiferromagnets where exact orthogonal arrangement of the magnetic moments is not governed by the isotropic superexchange, i.e., the tetragonal parent phases of electron-doped superconductors R_2CuO_4 (R = Nd, Pr, Sm). Here, the Cu magnetic moments in adjacent layers are oriented perpendicular to each other due to the anisotropic superexchange interaction.[10] For this class of materials, various sources of anisotropic contributions to the superexchange were investigated theoretically, including biquadratic superexchange[11] and pseudodipolar interactions.[12]

The magnitude and the sign of the magnetic interactions in edge-sharing and corner-sharing geometries in cuprates are quite different.[13] The leading isotropic superexchange of a 180° bond between two copper ions is strongly antiferromagnetic, while the leading order of a 90° superexchange is ferromagnetic and much weaker. In $Ba_3Cu_3In_4O_{12}$, the peculiar topology of the magnetic subsystem does not allow ascribing it to either of the above mentioned major classes. Similar to corner-sharing chains the CuO_4 units share only one vertex, but the Cu-O-Cu angle is close to 90° like in edge-sharing chains. According to our knowledge, neither any experimental study of the magnetic behavior nor calculations of magnetic exchange parameters in $Ba_3Cu_3In_4O_{12}$ have been undertaken so far.

$Ba_3Cu_3In_4O_{12}$ crystallizes in the tetragonal $I4/mcm$ space group with lattice parameters $a = 12.121(3)$ Å, $c = 8.511(4)$ Å, $V = 1250(2)$ Å^3, $Z = 4$, and $c/a = 0.70$.[14] The structure can be considered to be made of a perovskite-type network of InO_6 octahedra connected via vertices in three dimensions. Channels exist between these polyhedra that run parallel to the c axis containing either columns of Ba atoms or chains of vertex-sharing CuO_4 square planes. Within a column, there are two inequivalent crystallographic positions for copper (Cu^I and Cu^{II}) in a 1:2 proportion. Each Cu-O chain is rotated by 90° in the ab plane relative to its predecessor and the overall arrangement of the Cu-O chains is that of a square lattice, as shown in Fig. 1 (left panel). The Cu-O sublattice of $Ba_3Cu_3In_4O_{12}$ consists of highly unusual chains of square planar units seen for the cuprates in this structure type only. The members of this family are $Ba_3Cu_3In_4O_{12}$,[14] $Ba_3Cu_3Sc_4O_{12}$,[15] and their solid solutions.[15,16] In terms of coordination polyhedra, buckled Cu^IO_4 square units form vertex-sharing chains in which each square shares four vertices. The chains are constructed such that each buckled Cu^IO_4 square is bridged by two $Cu^{II}O_4$ concave squares linked via opposite oxygen corners of the Cu^IO_4 square. Each successive pair of concave $Cu^{II}O$ squares is rotated by 90° with respect to its predecessor along the c direction. This open linked chain, shown in Fig. 1 (right panel), could be described as a paper-chain motif.

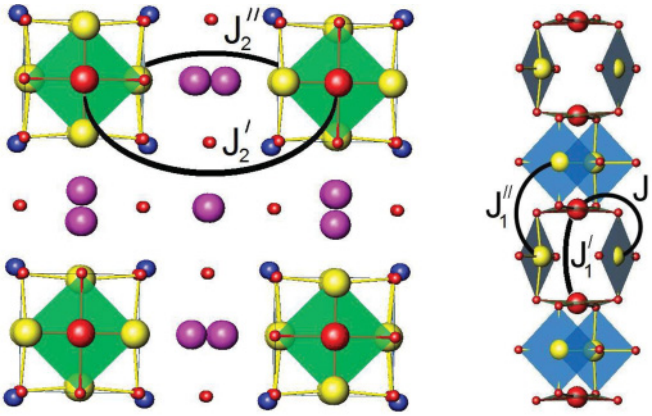

FIG. 1. (Color online) The $Ba_3Cu_3In_4O_{12}$ structure projected along the c axis. Large and medium isolated spheres represent the Ba^{2+} and the In^{3+} ions. Small spheres are the O^{2-} ions. The CuO_4 units are shown in polyhedral representation. The J_2' and J_2'' arcs mark Cu^{I}-Cu^{I} and Cu^{II}-Cu^{II} interchain exchange interactions, respectively (left panel). The paper-chain column consists of vertex-sharing buckled $Cu^{I}O_4$ (horizontal) and concave $Cu^{II}O_4$ (vertical) units. The J arc marks nearest-neighbor Cu^{I}-Cu^{II} exchange interaction. The J_1' and J_1'' arcs mark Cu^{I}-Cu^{I} and Cu^{II}-Cu^{II} next-nearest-neighbor intrachain exchange interactions, respectively (right panel).

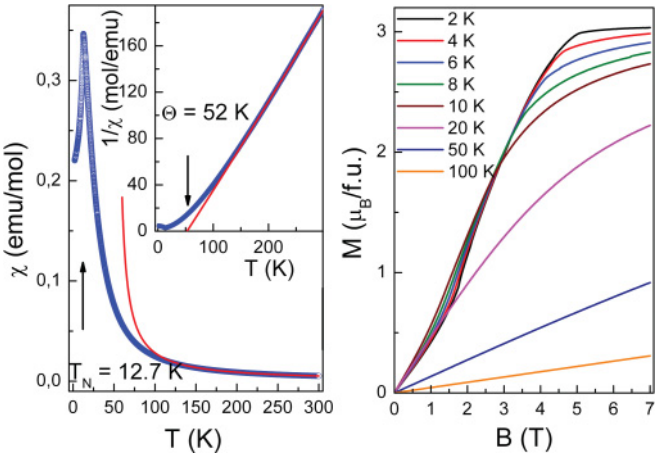

FIG. 2. (Color online) Magnetic susceptibility χ(T) of $Ba_3Cu_3In_4O_{12}$ taken at $B = 0.1$ T. The inset shows the temperature dependence of χ^{-1}. The solid lines represent the Curie-Weiss fit of the high-temperature data (left panel). The field dependencies of magnetization in $Ba_3Cu_3In_4O_{12}$. The fitting of M vs B curves by modified Brillouin function $B_{1/2}$ as described in the text gives number N of ferromagnetically correlated spins in paramagnetic state as 97 at 100 K, 151 at 50 K, and 208 at 20 K (right panel).

II. EXPERIMENT

Polycrystalline $Ba_3Cu_3In_4O_{12}$ was synthesized by means of a high-temperature solid state reaction of stoichiometric amounts of $BaCO_3$, CuO, and In_2O_3. These chemicals were ground, pelleted, and eventually fired in alumina crucibles at 850–950 °C in air for 72 h with regrinding every 24 h. Subsequently, the samples were quench cooled in air to room temperature. The phase purity of the sample obtained was confirmed by powder x-ray diffraction data collected using a "Radian-2" diffractometer with Cu K_α radiation over a 2θ range of 20°–60°. The field and temperature dependencies of the magnetization in $Ba_3Cu_3In_4O_{12}$ were measured in the temperature range 2–300 K and in magnetic fields up to 7 T by means of a "SQUID-VSM" magnetometer (Quantum Design). Specific heat data were obtained by a relaxation technique in a physical properties measurements system (PPMS, Quantum Design) in the temperature range 2–300 K on a sample with a mass of 12.7 mg. Electron spin resonance (ESR) experiments at high magnetic fields have been performed with a home-made frequency tunable ESR spectrometer on the basis of the Millimeterwave Vector Network Analyser from AB Millimetre.[17] The advantage of using sub-THz frequencies and correspondingly strong magnetic fields is the enhancement of the spectral resolution of an ESR experiment compared to conventional ESR spectroscopy usually confined to frequencies below 100 GHz.

III. RESULTS

The temperature dependence of the magnetic susceptibility $\chi = M/B$ in $Ba_3Cu_3In_4O_{12}$ taken at B = 0.1T is shown in Fig. 2 (left panel). At low temperatures, the sharp peak implies the formation of long-range antiferromagnetic order at $T_N = 12.7$ K. In the magnetically ordered state, the susceptibility drops by ~1/3 of its peak value, which is typical for polycrystalline easy-axis antiferromagnets. At high temperatures, the susceptibility follows a Curie-Weiss behavior and the data can be approximated by the sum of a temperature independent term $\chi_0 = -2.7 \times 10^{-4}$ emu/mol and the Curie-Weiss term $\chi_{CW} = C/(T - \Theta)$. Fitting the data yields $\Theta = 52$ K and $C = N_A g^2 \mu_B^2 S(S+1)/3k_B = 1.36$ emu K/mol, where N_A, μ_B, and k_B are the Avogadro, Bohr, and Boltzmann numbers, respectively. The value of the Curie constant gives a g factor $g = 2.2$. The obtained value of χ_0 is somewhat lower than the summation of Pascal's constants for the ions constituting $Ba_3Cu_3In_4O_{12}$: -3.3×10^{-4} emu/mol,[18] which is probably due to an additional temperature-independent van Vleck contribution of the Cu^{2+} ions. The positive value of the Weiss temperature Θ indicates the predominance of ferromagnetic coupling at high temperatures. However, there are significant deviations between the Curie-Weiss fit and the experimental data well above the actual long-range ordering temperature T_N as well as of the Weiss temperature Θ [see inset of Fig. 2 (left panel)]. These deviations indicate the increasing relevance of antiferromagnetic correlations upon cooling, which eventually yield the evolution of long-range antiferromagnetic order at T_N.

The field dependences of the magnetization M taken at selected temperatures in both the paramagnetic and the magnetically ordered state of $Ba_3Cu_3In_4O_{12}$ are shown in Fig. 2 (right panel). At $T = 100$ K, the magnetization depends practically linearly on the magnetic field up to 7 T. Upon lowering the temperature, however, these curves significantly deviate from linearity showing pronounced right-bending thereby qualitatively indicating a ferromagnetic-type behavior. In order to get further insight into the evolution of the spin correlations above T_N, we have analyzed the $M(B)$ curves using a modified Brillouin function $M(B) = M_S \tanh(N M_S B/k_B N_A T)$.[19] Here, M_S is the saturation moment of the nonlinear contribution

to *M(B)* which is described by the $B_{1/2}$ Brillouin function, N is the number of ferromagnetically correlated spins at a given temperature T. Fitting the data with M_S independent on the temperature and *N(T)* being the variable parameter provides a good description of the experimental data. At lowering temperature, the number N of correlated spins increases twice from 100 to 20 K, but it does not diverge approaching T_N. The increasing number of correlated spins upon cooling implies larger ferromagnetic correlation lengths at low temperature. Considering, on the other hand, the vicinity of long-range antiferromagnetic ordering at T_N, the data indicate either one- or two-dimensional ferromagnetic fluctuations emerging upon cooling while additional antiferromagnetic coupling yield long-range magnetic order below T_N. At the transition into the magnetically ordered state the *M(B)* curves acquire qualitatively new features at moderate magnetic fields. At lowest temperature, $T = 2$ K, the magnetization M reaches saturation of about 3.0 μ_B/f.u. (cf. with expected $M_S = 3.3\,\mu_B$/f.u. for g factor $g = 2.2$) in a modest magnetic field of about 5.2 T and does not change at further increase of a magnetic field.

The transition to the magnetically ordered state of $Ba_3Cu_3In_4O_{12}$ yields a quite pronounced anomaly in specific heat measurements, as shown in Fig. 3 (left panel). The main feature observed in $C_p(T)$ at $B = 0$ is the λ-type anomaly at T_N indicating a second-order phase transition. At T_N, the experimentally observed specific heat changes by $\Delta C_p = 5.15$ J/mol K. Although fluctuations affect the anomaly thereby increasing the anomaly size as compared to mean-field-like anomalies, this value is by far, i.e., ∼7.3 times, smaller than the expected jump size $\Delta C_{\text{magn}} = 5nRS(S+1)/[(S+1)^2+S^2] = 37.4$J/mol K in the mean-field model, with the number of magnetically active ions per formula unit $n = 3$, and the gas constant $R = 8.314$ J/mol K. In magnetic fields, the λ-type anomaly progressively smears

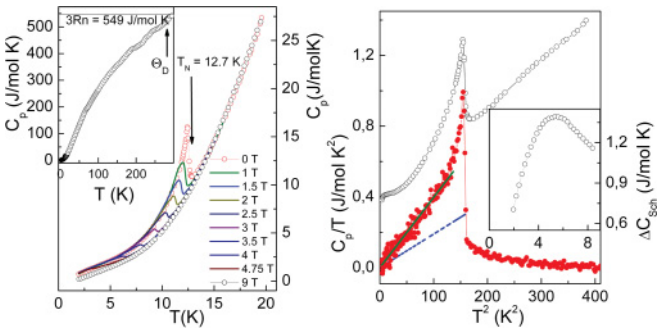

FIG. 3. (Color online) Temperature dependencies of the specific heat C_p in $Ba_3Cu_3In_4O_{12}$ taken under various magnetic fields. Inset: $C_p(T)$ measured up to room temperature. The deviations from a "smooth" behavior at elevated temperatures are due to the well-known influence of the Apiezon-N grease used to fix the sample in the specific heat puck of the PPMS device (left panel). The specific heat data in $Ba_3Cu_3In_4O_{12}$ in C_p/T vs T^2 representation (open symbols). The normalized Fisher's specific heat (solid symbols) is calculated from the experimental χ(T) data. The dotted and solid lines represent the phonon and magnon contributions at low temperatures, correspondingly. Inset: extra contribution to the specific heat at low temperatures of Schottky type (right panel).

out and shifts to lower temperatures, so that no singularity at the phase transition can be identified for $T \geqslant 2$ K and $B \geqslant 5$ T.

The inset to Fig. 3 (left panel) presents specific heat data measured up to room temperature. For $Ba_3Cu_3In_4O_{12}$, the Dulong-Petit value reaches $3Rz = 549$ J/mol K, with the number of atoms per formula unit $z = 22$. In the Debye model, about 0.95 of this value is reached at the Debye temperature Θ_D. In $Ba_3Cu_3In_4O_{12}$, this temperature amounts to ∼280 K. This allows approximating the phonon contribution to the heat capacity at low temperatures $C_{\text{ph}} = bT^3$ function with $b = 1.9 \times 10^{-3}$J/mol K^4.

The total entropy released at $T \leqslant T_N$ comprises various contributions and amounts to $\Delta S_{\text{total}} = 6.65$ J/mol K. The phonon part in this temperature range is $\Delta S_{\text{ph}} = 1.35$ J/mol K in accordance with the estimation of the Debye temperature. To separate the magnon contribution one has to calculate the Fisher's specific heat $\partial(\chi_{//}T)/\partial T$, where $\chi_{//}$ is the longitudinal magnetic susceptibility.[20] In polycrystalline easy-axis antiferromagnets, the magnetic susceptibility amounts to $\chi = \chi_{||}/3 + 2\chi_{\perp}/3$, where the transverse magnetic susceptibility $\chi_{\perp}$ is temperature independent at $T \leqslant T_N$. This behavior allows extracting the longitudinal susceptibility $\chi_{\parallel}$ from the experimental data χ(T) in $Ba_3Cu_3In_4O_{12}$ and, therefore, calculating the magnon contribution in the magnetically ordered state. The Fisher's specific heat $\partial(\chi_{//}T)/\partial T$ normalized to the experimental data of C_p at $T_N = 12.7$ K with account of phonon's contribution is shown in Fig. 3 (right panel).

Evidently, the magnon contribution, as expected for a 3D antiferromagnet, is $\sim aT^3$ with $a = 3.98 \times 10^{-3}$ J/mol K.[4] Thus we arrive at $\Delta S_{\text{magn}} = 2.67$ J/mol K. This value is ∼0.154 of the one estimated within the mean-field model $nR\ln(2S+1) = 17.29$ J/mol K and is in good agreement with the value of the jump size (∼0.137) in the specific heat at T_N. The extraction of both phonon ΔS_{ph} and magnon ΔS_{magn} contributions from the total entropy ΔS_{total} indicates that there is an extra contribution to the entropy $\Delta S_{\text{Sch}} = 2.63$ J/mol K. The specific heat corresponding to this extra contribution ΔC_{Sch} is shown in the inset of Fig. 3 (right panel). Basically, this nonmonotonous contribution is of a Schottky type, but a fit to the experimental data using $C_{\text{Sch}} \sim R(\Delta/T)^2\exp(\Delta/T)/[1+\exp(\Delta/T)]^2$ with $\Delta \sim 10$ K is rather poor due to numerous approximations needed to extract this term. Nevertheless, it can't be attributed to impurities since no indications for that are seen in the magnetic susceptibility data.

Typical ESR spectra of a powder sample of $Ba_3Cu_3In_4O_{12}$ at several selected temperatures that have been measured at an excitation frequency $\nu = 350$ GHz are shown in Fig. 4 (top panel). At a high temperature of 80 K, an asymmetric spectral shape is characteristic of the powder average of the anisotropic Cu^{2+} ESR signal.[21] This anisotropy is due to the g-factor tensor, which enters the resonance conditions $h\nu = g\mu_B B_{\text{res}}$. Here, B_{res} is the resonance field of the signal and h is the Planck constant. In a square planar ligand coordination of Cu^{2+} ions, which is the case for the $Ba_3Cu_3In_4O_{12}$ structure, one expects the g-factor value for the direction parallel to the normal to the CuO_4 square unit $g_{\parallel}$ to be larger than in the perpendicular direction, $g_{\perp}$,[22] i.e., $g_{\parallel} > g_{\perp} > 2$. Since the uniaxial symmetry axes of three CuO_4 square units in the unit cell are mutually

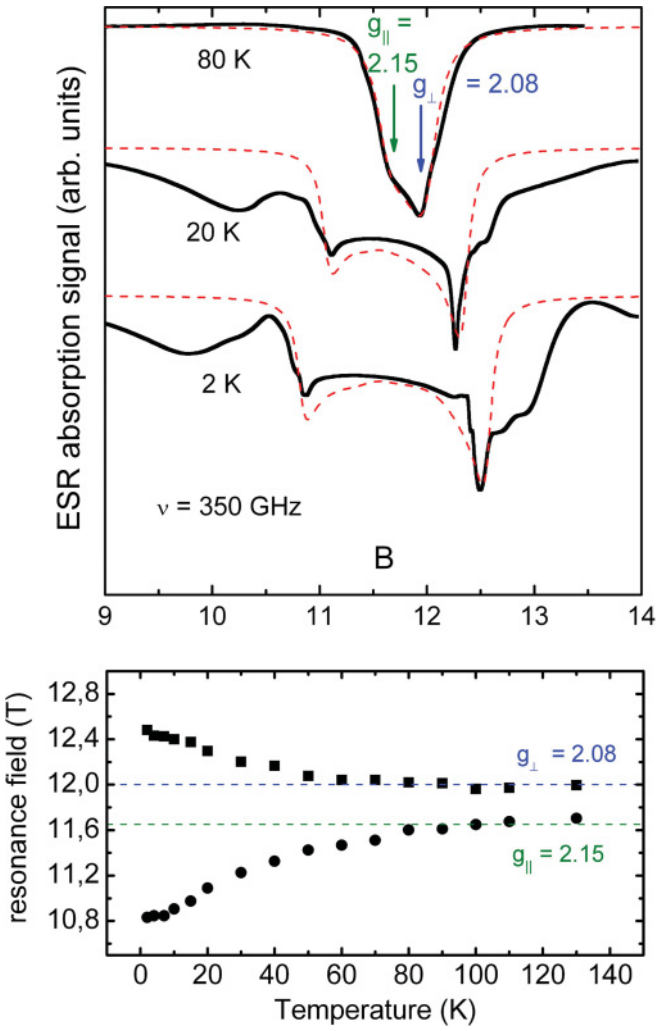

FIG. 4. (Color online) ESR spectra of a powder sample of $Ba_3Cu_3In_4O_{12}$ at $\nu = 350$ GHz for three selected temperatures 80, 20, and 2 K (top panel). Solid lines are experimental data, dashed lines are model spectra (see the text); temperature dependence of the resonance field corresponding to the peaks associated with the $g_\parallel$ and $g_\perp$ components of the g tensor. Dashed lines show the resonance field values $B_{\rm res} = h\nu/g\mu_{\rm B}$ which correspond to $g_\parallel = 2.15$ and $g_\perp = 2.08$ (bottom panel).

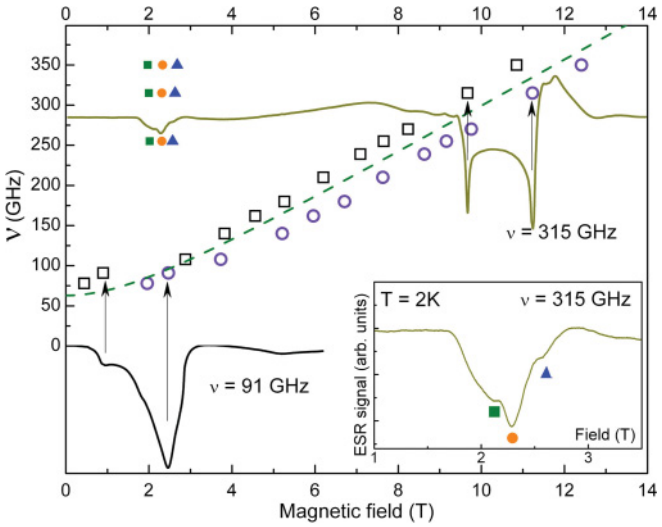

FIG. 5. (Color online) Frequency- magnetic field diagram of the ESR modes of a powder sample of $Ba_3Cu_3In_4O_{12}$ at $T = 2$ K. Open squares and circles correspond to the position of the peaks associated with the $g_\parallel$ and $g_\perp$ components of the g tensor. Exemplary ESR spectra at 315 and 91 GHz are shown for comparison. Dashed line models the gapped resonance branch $\upsilon^2 = \Delta^2 + (g\mu_{\rm B}B_{\rm res})^2$, which intersects the frequency axis at $\Delta = 63$ GHz (see the text). Inset shows the structured features that arise in the ESR spectrum at low fields at frequencies above ~250 GHz. The position of these features at several excitation frequencies is shown in the main panel by solid squares, circles, and triangles (see the text).

orthogonal, the corresponding g tensors should be mutually orthogonal as well. With this assumption the high-temperature powder averaged ESR spectrum of $Ba_3Cu_3In_4O_{12}$ can be well modeled yielding the principle values of the g-factor tensor $g_\parallel = 2.15$ and $g_\perp = 2.08$, as shown in Fig. 4 (top panel). In fact, the resonance field $B_{\rm res} = h\upsilon/g\mu_{\rm B}$ of the maximum absorption and the position of the shoulder on the left side of the ESR peak correspond closely to $g_\perp$ and $g_\parallel$, respectively, as indicated by arrows on Fig. 4 (top panel).

With lowering the temperature the ESR spectrum experiences a remarkable transformation. Its characteristic features associated with $g_\perp$ and $g_\parallel$ progressively split apart and get better resolved. The T dependence of corresponding resonance fields is shown in Fig. 4 (bottom panel). These features can be still reasonably well modeled assuming that the Cu spin at each mutually orthogonal Cu site is affected by an additional temperature-dependent anisotropic internal field [dashed lines in Fig. 4 (top panel)]. As can be seen in Fig. 4 (bottom panel) the resonance at the lowest measured temperature of 2 K is shifted by + 0.4 and –0.8 T for $g_\perp$ and $g_\parallel$ peaks, respectively. Remarkably, the growth of this internal field takes place in the temperature range where the development of antiferromagnetic (AFM) correlations becomes apparent in the static susceptibility data. Likely, the time scale of such correlations is longer than the time scale of the ESR experiment. Therefore the AFM correlations give rise to quasistatic internal fields from the viewpoint of ESR even in paramagnetic regime below ~70 K.

Apart from these peaks, additional broad absorption bands appear at the left and the right side of the low-temperature ESR spectrum shown in Fig. 4 (top panel). Their occurrence is probably associated with some distribution of internal fields and is prominent in the high-field regime only. In contrast, a well-defined double-peak structure of the ESR spectrum is robust with respect to the applied field and can be followed down to low fields. This is illustrated by the frequency versus magnetic field diagram obtained at $T = 2$ K, which is shown in Fig. 5. Here, the position of the peaks at various values of the excitation frequency ν is depicted by open squares and circles. The distance between the peaks is practically independent of the frequency and the field strength. These ESR excitations are obviously gapped. A modeling of the ν versus $B_{\rm res}$ dependence with a phenomenological relation $\upsilon^2 = \Delta^2 + (g\mu_{\rm B}B_{\rm res})^2$ shown by the dashed line agrees well with the experiment yielding the gap value $\Delta = 63$ GHz. Here the average g factor $g = (1/3)g_\parallel + (2/3)g_\perp$ has been used. Therefore, the model curve runs approximately in the middle

TABLE I. Basic parameters of the magnetic subsystem in selected quasi-one-dimensional compounds.

Compound	T_N, K	J, K	J_1, K	J_2, K	B_S, T	Comment
$LiCuVO_4$	2.3	–18	49	9	46.2	helix chain (Ref. 28)
Li_2CuO_2	9.4	–228	76	9	55.4	ferromagnetic chain (Ref. 25)
$Ba_3Cu_3In_4O_{12}$	12.7	–84	8	2	5.2	paper chain (present work)

between the data points corresponding to the two peaks. In fact, this relation holds for a "hard" direction of a uniaxial antiferromagnet.

IV. DISCUSSION

At first glance, $Ba_3Cu_3In_4O_{12}$ hardly seems anything but a three-dimensional easy-axis antiferromagnet. The predominance of ferromagnetic coupling at elevated temperatures in the paramagnetic state is in accordance with the assumption of the leading role of a ~90° bond Cu^{I}-O-Cu^{II} nearest-neighbor superexchange interaction $J < 0$ (cf. Fig. 1). However, strong deviation from the "ferromagnetic" Curie-Weiss law seen in this compound at low temperatures can be expected taking into account well-established frustrating influence of the next-nearest-neighbor superexchange interaction $J_1'' > 0$ through Cu^{II}-O-O-Cu^{II} bonds.[23] Depending on the frustration ratio $\alpha = J_1''/J$, the combined action of $(J,\ J_1'')$ interactions may result in the formation of either helix structures with various pitch angles at $\alpha \geqslant 0.25$ or ferromagnetic chains at $\alpha \leqslant 0.25$.[24] Moreover, the ferromagnetic chain arrangement may also survive at $\alpha \geqslant 0.25$ if it is stabilized by interchain interactions J_2''.[25]

The *naive* scenario for the long-range magnetic order in $Ba_3Cu_3In_4O_{12}$ is, therefore, that of ferromagnetic "paper-chain" columns, which are coupled antiferromagnetically. In this simplified model, $J_1' = J_1'' = J_1$ and $J_2' = J_2'' = J_2$. Then, in accordance with the mean-field formula, $g\mu_B B_S = 2zJ_2S$ for a spin $S = 1/2$, a g factor $g = 2.2$ and the number of interchain nearest-neighbors $z = 4$, the value of the determined saturation field $B_S = 5.2$ T (~ 3.5 K) defines the interchain exchange interaction parameter $J_2 \sim 2$ K. Through the simple expression $T_N = (|J| \times J_2)^{1/2}$ one can estimate the nearest-neighbor intrachain exchange interaction parameter $J = -84$ K. In the mean-field theory, the summation of exchange interaction parameters J_i is presumed for the Weiss temperature $\Theta = \Sigma_i z_i S(S+1)|J_i|/3$. Taking the intrachain nearest-neighbors number $z = 2$ and the intrachain next-nearest-neighbors number $z = 4$ one can get the value of the next-nearest-neighbor exchange interaction parameter within the chains $J_1 = 8$ K. This, in turn, gives the frustration ratio $a = J_1/J \sim 0.1$in accordance with the postulated scenario. Of course, significantly elaborated formula can be used to estimate the exchange interaction parameters J, J_1, and J_2 in quasi-one-dimensional systems within a modified mean-field theory.[26,27] For given values of the saturation field $B_S \sim 5.2$ T and the Neel temperature $T_N = 12.7$ K, all of them result in even smaller values of J_1/J and J_2/J ratios.

However, the apparent triumph of the mean-field theory for the case of antiferromagnetically coupled ferromagnetic chains is quite doubtful, if to compare $Ba_3Cu_3In_4O_{12}$ with any other quasi-one-dimensional compound and consider the minute details of the available data. Taking as representative the helix chain compound $LiCuVO_4$[28] and the ferromagnetic chain compound Li_2CuO_2,[25] one may notice the striking disparity with $Ba_3Cu_3In_4O_{12}$ regarding interrelations of the magnetic ordering temperature T_N, the saturation field B_S, and the exchange interaction parameters J_i, as given in Table I. Evidently, the magnetic field B_S necessary to saturate the magnetization in both helix and ferromagnetic chain compounds is by an order of magnitude larger than in paper-chain compound despite the relatively high magnetic ordering temperature T_N in the latter.

The low value of the saturation field in $Ba_3Cu_3In_4O_{12}$ is not only a special feature of the magnetization curves in this compound, sharp additional singularities are seen at several critical fields for $T < T_N$. As shown in Fig. 6 (left panel), the derivatives dM/dB of the magnetization curves taken at $T < T_N$ highlight these features, i.e., peaks at B_1 and B_2, a sharp change of slope at B_3 and full saturation at B_4. The magnetization curves taken at low temperatures can be modeled quantitatively if one presumes the magnetic moments of Cu^{I} and Cu^{II} ions forming separate magnetic subsystems and experiencing the spin-flop and spin-flip transitions independently. The satisfactory fit of the experimental data is obtained ascribing B_1 and B_4 to spin-flop and spin-flip transitions in the Cu^{II} subsystem and B_2 and B_3 to spin-flop and spin-flip transitions in the Cu^{I} subsystem, correspondingly. In the mean-field approximation $B_{flop} = (2B_A B_E - B_A^2)^{1/2}$ and $B_{flip} = B_E$,

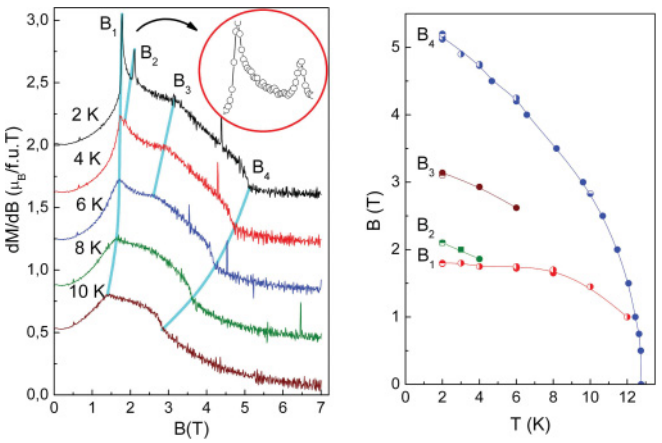

FIG. 6. (Color online) The derivatives of the magnetization dM/dB of $Ba_3Cu_3In_4O_{12}$. The subsequent dM/dB curves are shifted with respect to each other. Solid lines are guides to the eye to follow the subsequent spin-flop and spin-flip transitions. The inset represents the enlarged region of spin-flop transitions (left panel). The B-T magnetic phase diagram in $Ba_3Cu_3In_4O_{12}$ as compiled from the specific heat C_p and magnetization M data (right panel).

where B_A is the anisotropy and B_E is the exchange fields. Using our experimental values for the critical fields, we arrive at $B_A^I = 0.8\,T$, $B_E^I = 3.15\,T$ and $B_A^{II} \sim 0.3\,T$, $B_E^{II} \sim 5.2\,T$.

Overall, this points to a possible decoupling in the magnetic subsystem of $Ba_3Cu_3In_4O_{12}$. At increasing temperatures, the *M(B)* curves smooth out reaching the standard Brillouin function, but the progressively smeared anomalies at the spin-flop-like and spin-flip-like transitions persist. This is summarized in the magnetic phase diagram, which is constructed from the magnetization M and specific heat C_p data, as shown in Fig. 6 (right panel). The B_1 and B_2 lines in this diagram correspond to spin-flop transitions in Cu^{II} and Cu^{I} subsystems [note, the ~2:1 ratio in magnitude of subsequent singularities, as shown in the inset to Fig. 4 (left panel)], while the B_3 and B_4 lines denote spin-flip transitions in Cu^{I} and Cu^{II} subsystems.

Additional evidence for the presence of multiple phase boundaries in $Ba_3Cu_3In_4O_{12}$ can be derived from the ESR measurements. The excitation gap $\Delta = 63$ GHz, which arises in the AFM ordered state due to magnetic anisotropy enables an estimate of the corresponding spin flop field $B_{flop} = h\Delta/g\mu_B \approx 2.15\,T$. This value is somewhat larger than the spin flop field B_1 and is close to the spin flop field B_2, both determined in the static magnetization measurements. This correspondence gives additional evidence that both the static and dynamic magnetic response originate from the same spin system. Approximately, in the same field range where magnetization measurements reveal a sequence of spin reorientations at fields B_1, B_2, and B_3, a peculiar structure comprising a peak with two shoulders is visible in the ESR spectrum (see inset in Fig. 5). In fact, these features are most likely of a nonresonance nature since their position is practically independent of the excitation frequency (see solid squares, circles, and triangles in the ν-B diagram in Fig. 5). However, they are only seen above a certain threshold frequency of about ~250 GHz, suggesting a dynamic origin of this effect. Tentatively, it might be associated with some changes of the nonresonant microwave absorption in the sample upon spin reorientation.

The decoupling in the magnetic subsystem in $Ba_3Cu_3In_4O_{12}$ is only possible for an orthogonal spin arrangement of the copper ions. Such highly unusual magnetic structure can be formed to avoid heavy frustration of exchange interactions in $Ba_3Cu_3In_4O_{12}$. The frustration of ferromagnetic nearest-neighbor Cu^{I}-O-Cu^{II} interactions by antiferromagnetic next-nearest-neighbor Cu^{II}-O-O-Cu^{II} interactions is not the only factor influencing the formation of three-dimensional long-range order in $Ba_3Cu_3In_4O_{12}$. The intrachain Cu^{II}-Cu^{II} interaction within the columns is intrinsically frustrated itself due to the tetrahedral arrangement of Cu^{II} ions. Moreover, the interchain interaction within the Cu^{II} subsystem is frustrated, too. As shown in Fig. 7, the presumably decoupled copper subsystem in $Ba_3Cu_3In_4O_{12}$ consists of a three-dimensional rectangular Cu^{I} network (left panel) embedded between mutually orthogonal Cu^{II} two-dimensional Shastry-Sutherland layers (right panel), resulting in a three-dimensional heavily frustrated Shastry-Sutherland system.[29] In generalized Shastry-Sutherland model the dimers on neighboring layers have no direct coupling, but couple to an intermediate spin between them.[30]

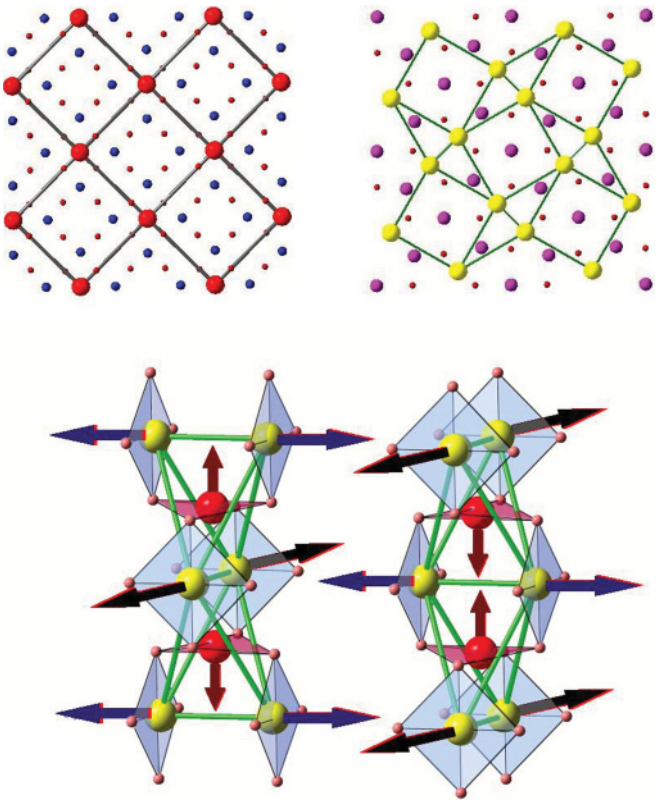

FIG. 7. (Color online) The structure of Cu^{I} layers (left panel) and Cu^{II} layers (right panel) in the *ab* plane in $Ba_3Cu_3In_4O_{12}$. The Cu^{2+} ions are interconnected by solid lines. The large, medium, and small size isolated spheres represent Ba^{2+}, In^{3+}, and O^{2-} ions, respectively. Note that the adjacent Cu^{II} layers are rotated by 90° with respect to each other along the c axis. The orthogonal spin arrangement of copper magnetic moments as possible ground state of generalized three-dimensional Shastry-Sutherland network in $Ba_3Cu_3In_4O_{12}$ (bottom panel).

For the Shastry-Sutherland model, it is clear that the system will exhibit long-range Neel order at predominance of interdimer interaction, and will be in the short-range dimer state at prevalence of intradimer interaction. Recent studies suggest that there exists an intermediate phase between the Neel phase and the dimer phase.[31] While the nature of a possible intermediate state in three-dimensional Shastry-Suthertland model remains an open question, one possible candidate could be an orthogonal antiferromagnetic network.[32]

V. CONCLUSION

In our view, the ground state in $Ba_3Cu_3In_4O_{12}$ is comprised of three virtually independent orthogonal subsystems, as shown in Fig. 7 (bottom panel). No frustration is present in this arrangement. The weakness of relevant exchange interactions results in rather low value of B_S, while the absence of frustration in the orthogonal spin arrangement leads to a relatively high T_N. In this structure, favored by magnetocrystalline anisotropy, pseudodipolar, and Dzyaloshinskii-Moriya interactions, quantum fluctuations provide the coupling between mutually orthogonal magnetic subsystems

resulting in an impressive "order-by-disorder" effect. The Schottky-type anomaly in the specific heat may define the energy of stabilization of the quantum ground state in this system. The low magnetic field necessary to saturate the magnetization in $Ba_3Cu_3In_4O_{12}$ tentatively indicates the proximity of this system to a quantum critical point separating orthogonal and collinear phases.

While the neutron scattering experiment on $Ba_3Cu_3In_4O_{12}$ is hampered by high absorption cross section of indium, the recently performed neutron diffraction study on isostructural compound $Ba_3Cu_3Sc_4O_{12}$ has revealed complex magnetic order at low temperatures, which is greatly influenced by external magnetic field.[33] The analysis of available data on $Ba_3Cu_3Sc_4O_{12}$ allows excluding ferromagnetic "paper-chain" model for this compound. There are no magnetic reflections corresponding to this arrangement, while the magnetic reflection with propagation vector $\mathbf{k} = [010]$ is compatible with orthogonal antiferromagnetic network. It does not allow, however, to distinguish between collinear and orthogonal antiferromagnetic structures. Our measurements of thermodynamic properties of $Ba_3Cu_3Sc_4O_{12}$ ($T_N = 16$ K) show its full similarity to $Ba_3Cu_3In_4O_{12}$ making, therefore, these compounds a new family of noncollinear antiferromagnets.

Concluding, the magnetic subsystem in $Ba_3Cu_3In_4O_{12}$ seems to be frustrated in every sector regarding intrachain and interchain interactions. The formation of an orthogonal spin structure lifts all these multiple frustrations. In accordance with the orthogonal arrangement of copper magnetic moments, the Cu^{I} and Cu^{II} subsystems are to be decoupled and the Cu^{II} subsystem decouples into two equivalent sub-sub-systems itself. This is in agreement with the observation of two distinct spin-flop-like and two distinct spin-flip-like transitions of different magnitudes. In case of exclusion of the isotropic superexchange interaction in our consideration, other weak, basically anisotropic interactions masked in helix and collinear antiferromagnets manifest themselves, making $Ba_3Cu_3In_4O_{12}$ a new and excellent playground to study the physics of low-dimensional and frustrated quantum spin systems.

ACKNOWLEDGMENTS

We acknowledge the support of the present work by Deutsche Forshungsgemeinshaft Grants DFG 486 RUS 113/982/0-1, FOR 912, and WO 1532/3-1, Russian Foundation for Basic Research Grants 10-02-00021, 11-02-00083, and Russian Ministry of Science and Education State Contracts 11.519.11.6012, 14.740.11.1365.

[1] M. Jaime, V. F. Correa, N. Harrison, C. D. Batista, N. Kawashima, Y. Kazuma, G. A. Jorge, R. Stern, I. Heinmaa, S. A. Zvyagin, Y. Sasago, and K. Uchinkura, Phys. Rev. Lett. **93**, 087203 (2004).

[2] M. Hase, I. Terasaki, and K. Uchinokura, Phys. Rev. Lett. **70**, 3651 (1993).

[3] J. Darriet and L. P. Regnault, Solid State Comm. **86**, 409 (1993).

[4] H. Kageyama, K. Yoshimura, R. Stern, N. V. Mushnikov, K. Onizuka, M. Kato, K. Kosuge, C. P. Slichter, T. Goto, and Y. Ueda, Phys. Rev. Lett. **82**, 3168 (1999).

[5] T. Masuda, A. Zheludev, B. Roessli, A. Bush, M. Markina, and A. Vasiliev, Phys. Rev. B **72**, 014405 (2005).

[6] M. Enderle, C. Mukherjee, B. Fåk, R. K. Kremer, J.-M. Broto, H. Rosner, S.-L. Drechsler, J. Richter, J. Malek, A. Prokofiev, W. Assmus, S. Pujol, J.-L. Raggazzoni, H. Rakoto, M. Rheinstädter, and H. M. Rønnow, Europhys. Lett. **70**, 237 (2005).

[7] Y. Tarui, Y. Kobayashi, and M. Sato, J. Phys. Soc. Jpn. **77**, 043703 (2008).

[8] S.-L. Drechsler, J. Richter, R. Kuzian, J. Malek, N. Tristan, B. Büchner, A. S. Moskvin, A. A. Gippius, A. Vasiliev, O. Volkova, A. Prokofiev, H. Rakoto, J.-M. Broto, W. Schnelle, M. Scmitt, A. Ormeci, C. Loison, and H. Rosner, J. Magn. Magn. Mater. **316**, 306 (2007).

[9] R. Bursill, G. A. Gehring, D. J. J. Farnell, J. B. Parkinson, Tao Xiang, and Chen Zeng, J. Phys.: Condens. Matter **7**, 8605 (1995).

[10] R. Sachidanandam, T. Yildirim, A. B. Harris, A. Aharony, and O. Entin-Wohlman, Phys. Rev. B **56**, 260 (1997).

[11] L. X. Hayden, T. A. Kaplan, S. D. Mahanti, Phys. Rev. Lett. **105**, 047203 (2010).

[12] D. Petitgrand, S. V. Maleev, Ph. Bourges, and A. S. Ivanov, Phys. Rev. B **59**, 1079 (1999).

[13] S. Tornow, O. Entin-Wohlman, and A. Aharony, Phys. Rev. B **60**, 10206 (1999).

[14] L. E. Aleandri and H. G. von Schnering, J. Less-Common Met. **156**, 181 (1989).

[15] D. H. Gregory, P. R. Mawdsley, S. J. Barker, W. Daniell, and D. P. Weston, J. Mater. Chem. **11**, 806 (2001).

[16] A. L. Kharlanov, N. R. Khasanova, M. V. Paromova, E. V. Antipov, L. N. Lykova, and L. M. Kovba, Zh. Neorg. Khim. (in Russian) **35**, 3067 (1990).

[17] C. Golze, A. Alfonsov, R. Klingeler, B. Büchner, V. Kataev, C. Mennerich, H.-H. Klauss, M. Goiran, J.-M. Broto, H. Rakoto, S. Demeshko, G. Leibeling, and F. Meyer, Phys. Rev. B **73**, 224403 (2006).

[18] G. A. Bain and J. F. Berry, J. Chem. Educ. **85**, 532 (2008).

[19] R. Klingeler, B. Büchner, S.-W. Cheong, and H. Hücker, Phys. Rev. B **72**, 104424 (2005).

[20] M. E. Fisher, Phil. Mag. **7**, 1731 (1962).

[21] C. P. Poole, *Electron spin resonance: A comprehensive treatise on experimental techniques* (Dover, Mineola, New York, 1996).

[22] Abragam and B. Bleaney, *Electron Paramagnetic Resonance of Transition Ions* (Clarendon, Oxford, 1970).

[23] S.-L. Drechsler, O. Volkova, A. N. Vasiliev, N. Tristan, J. Richter, M. Schmitt, H. Rosner, J. Málek, R. Klingeler, A. A. Zvyagin, and B. Büchner, Phys. Rev. Lett. **98**, 077202 (2007).

[24] M. Schmitt, J. Malek, S.-L. Drechsler, and H. Rosner, Phys. Rev. B **80**, 205111 (2009).

[25] W. E. A. Lorenz, R. O. Kuzian, S.-L. Drechsler, W.-D. Stein, N. Wizent, G. Behr, J. Málek, U. Nitzsche, H. Rosner, A. Hiess, W. Schmidt, R. Klingeler, M. Loewenhaupt, and B. Büchner, Europhys. Lett. **88**, 37002 (2009).

[26] H. J. Schulz, Phys. Rev. Lett. **77**, 2790 (1996).

[27]V. Yu. Irkhin and A. A. Katanin, Phys. Rev. B **55**, 12318 (1997).
[28]N. Buettgen, H.-A. Krug von Nidda, L. E. Svistov, L. A. Prozorova, A. Prokofiev, and W. Assmus, Phys. Rev. B **76**, 014440 (2007).
[29]B. S. Shastry and B. Sutherland, Physica B **108**, 1069 (1981).
[30]S. Chen and H. Buettner, Eur. Phys. J. B **29**, 15 (2002).
[31]W. Zheng, J. Oitmaa, and C. J. Harner, Phys. Rev. B **65**, 014408 (2001).
[32]D. Carpentier and L. Balents, Phys. Rev. B **65**, 024427 (2001).
[33]A. V. Mahajan, B. Koteswara Rao, and J. Bobroff, Bull. Am. Phys. Soc. **54**, 06.14.7 (2009); V. Siruguri, P. D. Babu, and A. V. Pimpale, UGC-DAE CSR Bulletin **19**, 5 (2010).